A 3-dimensional micro- and nanoparticle transport and filtration model (MNM3D) applied to the migration of carbon-based nanomaterials in porous media

A 3D model for the simulation of particle transport in porous media. MNM3D applied to carbon-based nanomaterials

Carlo Bianco[1], Tiziana Tosco[1], Rajandrea Sethi[1]

[1] *Politecnico di Torino – DIATI – C.so Duca degli Abruzzi 24, 10129 - Torino, Italy*

carlo.bianco@polito.it, tiziana.tosco@polito.it, rajandrea.sethi@polito.it

Original Citation:
C. Bianco, T. Tosco, R. Sethi (2016), A 3-dimensional micro- and nanoparticle transport and filtration model (MNM3D) applied to the migration of carbon-based nanomaterials in porous media. Journal of Contaminant Hydrology 193, pp. 10-20. - ISSN 0169-7722

Availability:
This version is available at: http://porto.polito.it/2647425/
since: May 2017

Publisher:
Elsevier

Published version:
DOI: 10.1016/j.jconhyd.2016.08.006

A 3D model for the simulation of particle transport in porous media. MNM3D applied to carbon-based nanomaterials

Carlo Bianco[1], Tiziana Tosco[1], Rajandrea Sethi[1]

[1] *Politecnico di Torino – DIATI – C.so Duca degli Abruzzi 24, 10129 - Torino, Italy*

carlo.bianco@polito.it, tiziana.tosco@polito.it, rajandrea.sethi@polito.it

Journal of Nanoparticle Research 19(3), Art. n. 107

DOI: 10.1007/s11051-017-3814-x

DIATI (Department of Land, Environment and Infrastructure Engineering)

Politecnico di Torino, C.so Duca degli Abruzzi 24, Torino 10129, Italy

* Corresponding Author: phone +39-011-090-7735; fax: +39-011-090-7699; e-mail:

rajandrea.sethi@polito.it

1 Keywords

Colloid transport in porous media, numerical modeling, carbon-based nanoparticles, field-scale transport simulation

2 Abstract

The potential impacts of engineered nanoparticles (NPs) on the environment in general, and on groundwater in particular, is increasing over years. NPs in the environment can act both as contaminants, when they are unintentionally released, and as remediation agents when injected on purpose at contaminated sites. In this work two carbon-based NPs are considered, namely CARBO-IRON®, a new material developed for contaminated site remediation, and single layer graphene oxide (SLGO), a potential contaminant of the next future. For CARBO-IRON® it is crucial to understand how it is transported during injection in the contaminated aquifer, while for SLGO the focus is the long-term transport once released in the subsurface. Understanding and modelling the transport and deposition of such NPs in aquifer systems is a key aspect in both cases, and numerical models capable to simulate NP transport in groundwater in complex 3D scenarios are necessary. To this aim, this work proposes a modeling approach based on modified advection-dispersion-deposition equations accounting for the coupled influence of flow velocity and ionic strength on particle transport. A new modelling tool (MNM3D - Micro and Nanoparticles transport Model in 3D geometries) is presented for the simulation of NPs injection and transport in 3D scenarios. MNM3D is based on the well-known transport model RT3D (Clement et al. 1998). Two simulations of NP transport at a large scale are presented, namely the simulation of a pilot-scale injection of CARBO-IRON® in a 2D confined tank, and a full scale 3D simulation of SLGO release and long-term transport in a heterogeneous aquifer. MNM3D showed to potentially represent a valid tool for the prediction of the long-term behaviour of engineered nanoparticles released in the environment (eg. from landfills), and the preliminary design of in situ aquifer remediation through injection of suspensions of reactive NPs.

3 Introduction

Engineered nanoparticles (NPs) are largely employed in industrial processes and for the manufacturing of many commercially available products (e.g. sunscreen, food additives, etc.). Their use and hence their presence in the environmental matrices is likely to increase in the future (Li et al. 2006). In most cases, the release in the environment is an undesired consequence, while in fewer cases the NPs are introduced into the environment on purpose, eg. for groundwater remediation (eg. nanoparticles injected at contaminated sites). In both cases, a significant role is played by carbon-based materials, which generally present peculiar properties potentially affecting their mobility in the environmental compartments, compared to other engineered nanomaterials.

Nanosized particles used in industrial processes and commercial products can be released into the environment and, in particular, into groundwater throughout their entire life cycle, thus representing a real risk for human health (Tratnyek and Johnson 2006). Once released, nanoparticles can exhibit inherent toxicity, or play a role in enhancing the mobility of many contaminants (Bekhit and Hassan 2007), acting as a mobile solid phase which accelerates the transport of strongly sorbing contaminants (colloid-facilitated contaminant transport) (Ryan and Elimelech 1996). In particular, graphene, graphene oxide and graphene-containing materials may represent a potential concern in this sense. Research on graphene has grown substantially in recent years, thanks to the unique properties of this material. A broad range of graphene-based nanomaterials, including pure single-layer graphene, graphene oxide (GO), and several functionalized graphenes are routinely synthesized. Several industrial applications of graphene-based NPs are promising but still at a basic research stage, while others (eg. paintings and coating) are on the way of the scale-up to industrial level, and graphene-based products are expected to be on the market (and consequently in the environment) in only few years (Novoselov et al. 2012). Pure graphene and several other graphene-based NPs are hydrophobic, and therefore their mobility in the subsoil is very limited. Conversely, hydrophilic derivatives, like GO and most functionalized graphenes, are potentially very mobile in saturated porous media, as already evidenced in the literature (Feriancikova and Xu 2012, Lanphere et al. 2013, Liu et al. 2013b). Moreover, their strong sorbing capacity may also represent an additional potential risk in facilitating the transport of poorly soluble contaminants. It is therefore extremely important to develop approaches and tools able to predict the long-term fate of these emerging contaminants and the potential associated risk.

The second environmental implication of the development of engineered NPs involves their use for groundwater remediation. Several engineered NPs have been studied to this purpose in the last years, e.g. microscale and nanoscale zero-valent iron particles (MZVI, NZVI) (Zhang 2003, O'Carroll et al. 2013, Yan et al. 2013, Tosco et al. 2014b), carbon/iron composites (Mackenzie et al. 2012, Mackenzie et al. 2015), and nanosized iron oxides (Bosch et al. 2010, Braunschweig et al. 2013). In particular, nanoscale zerovalent iron

has been investigated at laboratory and field scale both in the form of NZVI particles alone and as composite materials like CARBO-IRON®, where NZVI is embedded in a carbon matrix to promote mobility and contaminant targeting (Mackenzie et al. 2012, Mackenzie et al. 2015). NZVI proved to be very effective in degrading a wide range of recalcitrant contaminants (e.g. chlorinated hydrocarbons, etc.) (Li et al. 2006, Tratnyek and Johnson 2006). However, despite the large potential of nanoparticle-based remediation technologies, there are still particular concerns, especially related to the particle mobility, that must be addressed in regard to the effectiveness and feasibility in field-scale applications.

Understanding and modelling the transport and the deposition of colloidal particles in saturated porous media is therefore a key aspect both in the short-term (design of a field-scale injection) and the long-term (spreading in the environment) prediction of particle distribution. The mobility of nanoparticles in saturated porous media is determined by the combination of particle-particle and particle-porous medium physico-chemical interactions, which typically result in dynamic deposition and release phenomena. The kinetic coefficients governing these processes have been proven to be strongly influenced by both hydrodynamic (e.g. pore-water velocity, injection flow-rate) (Tufenkji and Elimelech 2004a, Bradford and Torkzaban 2008) and hydrochemical parameters (e.g. pore-water ionic strength, pH) (Saleh et al. 2008, Tosco et al. 2009). In this work, a specific focus is posed on modeling the influence of temporal and spatial variations of flow velocity and ionic strength. A correct modeling of the effects of spatial variations of flow velocity is relevant for practical applications in which it can be considered as a design parameter, such as the remediation of polluted groundwater by injection of engineered nanoparticle slurries via wells or direct push techniques (Tosco et al. 2014a). On the other hand, the geochemical properties, particularly the ionic strength (IS), have a strong influence on the long-term behavior of colloidal particles under the natural flow field (e.g. release of anthropogenic nanoparticles into groundwater, post-remediation fate of injected particles). It is therefore crucial to incorporate the influence of both parameters in a 3D modeling approach to particle transport.

Several analytical and numerical tools have been developed to model the transport of NPs in groundwater (Šimůnek et al. 2008, Tosco and Sethi 2009, Katzourakis and Chrysikopoulos 2014, Becker et al. 2015). In general, NP transport is modeled by a set of partial differential equations (PDE) describing the attachment and detachment of the particles onto and from the porous medium. Particle interaction with soil matrix is a complex phenomenon controlled by a number of variables, including specific properties of the particles (e.g., size, shape, surface charge), the soil (e.g., grain composition, presence of organic matter), pore water (e.g., ionic species and concentrations) and the hydrodynamics (flow velocity, permeability, etc.). These variables can be coupled with the constitutive equations which express the dependency of the particle deposition and release kinetics on the IS and the pore-water velocity. To this aim, the numerical tool MNMs was recently released for the simulation of colloidal transport in 1D Cartesian (Tosco and Sethi 2009) and radial (Tosco et al. 2014a) coordinates, solving IS- and velocity-dependent transport of colloidal particles.

However, it is worth to highlight that all equations, relationships and attachment/detachment kinetics usually adopted for the description of the interactions between particles and porous medium have been developed for "typical" colloids, with a spherical or at least partly regular shape (eg. model latex spheres, viruses and bacteria, and at a partial extent NZVI). This is not the case of particles having one or two significantly predominant size, like graphene-based nanomaterials, which are similar to thin sheets, or CARBO-IRON®, which presents a very irregular shape. Moreover, a second critical issue is that, until now, such complex interaction phenomena have been mainly tackled in domains which have simplified geometry and boundary conditions, while modeling of full scale particle transport under complex geo-chemical and hydrodynamic scenarios is still an open issue. Despite the existence of advanced models for the simulation of colloid transport in one-dimensional domains, the above mentioned large-scale applications require the development of full 3D numerical codes. To the authors' knowledge, few simulation tools are available in the literature for 3D colloid transport (Šimůnek et al. 2008, Johnson et al. 2013, Katzourakis and Chrysikopoulos 2014, Becker et al. 2015), and none of them implements direct correlations accounting for variations of groundwater IS and flow velocity.

In this work, the transport of two carbon-based nanomaterials having relevant environmental implications, namely CARBO-IRON® and single layer graphene oxide (SLGO), is assessed at a large scale. For CARBO-IRON®, the target is the simulation of field-scale injection, and consequently particular attention is devoted in modeling the particle transport under strong variations of flow velocity. For SLGO, the target is the long-term behavior in aquifer systems under natural flow and in a complex hydrodynamic and hydrochemical scenario, representing an unintentional release of SLGO in the subsoil.

To overcome the two issues discussed above (namely the suitability of existing modeling approaches for the two carbon-based materials, and the development of a modeling tool for the transport simulation in complex 3D domains), the present study proposes a new modeling tool, MNM3D, for the simulation of injections and transport of nanoparticle suspensions in generic complex scenarios. MNM3D, standing for Micro and Nanoparticles transport Model in 3D geometries, is a modified version of the well-known transport model RT3D (Clement 1997, Clement et al. 1998). In MNM3D the colloid transport equations and the dependencies of the attachment and detachment kinetic coefficients on transients in pore water IS and velocity have been implemented. Two applications of MNM3D to carbon-based NPs are presented here. MNM3D is first used to model a 2D pilot scale injection of CARBO-IRON®, where NP injection is dominated by velocity-dependent transport. In the second part of the paper, the suitability colloid transport equations for SLGO is verified against experimental data of column transport tests, and the results are up-scaled to simulate a spill of waste water containing SLGO in a heterogeneous 3D aquifer system.

4 Material and methods

4.1 Mathematical model

The transport of colloidal particles in saturated porous media is usually modeled using a modified advection-dispersion equation, which describes the dual-phase non-equilibrium interactions between particles in the liquid (water) and solid (grains) phase (Tosco et al. 2009, Chrysikopoulos et al. 2012, Katzourakis and Chrysikopoulos 2014). For a generic domain:

$$\begin{cases} \frac{\partial}{\partial t}(\epsilon C) + \sum_i \frac{\partial}{\partial t}(\rho_b S_i) + \frac{\partial}{\partial x_i}(q_i C) - \frac{\partial^2}{\partial x_i^2}(\epsilon D_{ij} C) - q_s C = 0 \\ \frac{\partial}{\partial t}(\rho_b S_i) = f(C, S_i) \end{cases} \quad (1)$$

where ϵ is the porosity of the medium [-], q_i is the Darcyan flow velocity along the ith direction [L T^{-1}], C is the colloid concentration in the mobile phase [M L^{-3}], S is the colloid concentration in the solid phase [M M^{-1}], D_{ij} the dispersion coefficient tensor [L^2 T^{-1}], ρ_b is the bulk density of the solid matrix [M L^{-3}], and q_s is the volumetric flow rate per unit volume of aquifer [T^{-1}]. The second term in eq. 1 represents the exchange between liquid and solid phase due to particle deposition and release.

As a general rule, more than one concurrent mechanism can take place at the same time, and consequently the total particles concentration in the solid phase S is the sum of the concentrations resulting for individual deposition mechanisms, $S = S_1 + S_2 + \ldots$ In many cases, deposition is controlled by both physical (mechanical filtration and/or straining) and physical-chemical mechanisms, and two interaction sites are therefore requested in eq. 1.

A general formulation for the exchange term between liquid and solid phase was proposed by the authors in a previous work (Tosco and Sethi 2010):

$$\frac{\partial}{\partial t}(\rho_b S_i) = \epsilon k_{a,i}\left(1 + A_i S_i^{B_i}\right) C - \rho_b k_{d,i} S_i \quad (2)$$

where $k_{a,i}$ and $k_{d,i}$ are respectively the attachment and detachment coefficients [T^{-1}], A_i and B_i are the multiplier [-] and exponent [-] for the general kinetic formulation of colloid deposition. The equation can be adapted to most formulations of deposition and release mechanisms, including linear deposition typical of early-stage particle transport ($A_i = 0$), and non-linear deposition processes, typical of late-stage deposition. The latter arise when the transport of suspended particles is influenced by the presence of the deposited ones, and include blocking ($A_i = -\frac{1}{s_{max,i}} < 0,\ B_i = 1$), observed when the deposition rate decreases with increasing S_i, and ripening ($A_i > 0$), observed when deposition rate increases with increasing S_i.

The influence of the groundwater ionic strength and flow velocity on the nanoparticle transport has been extensively studied in the literature, both individually or as concurrent mechanisms (Bradford et al. 2009), particularly at the pore scale. However, at larger scales, despite several correlations have been proposed to independently model these phenomena, to the authors' knowledge no modelling tools have yet been developed to take into account the coupled effect of IS and flow velocity variations on both deposition and release of NPs.

Increasing groundwater IS typically results in a reduced the repulsion between particles and porous medium, and consequently in an increased deposition rate (Ryan and Elimelech 1996, Tufenkji and Elimelech 2004b, Tiraferri et al. 2011). Conversely, a large quantity of deposited particles can be suddenly released from the porous medium in the case of flushing with fresh water, thus giving rise to potential secondary sources of particles (Kanti Sen and Khilar 2006). The effects of changes in salt concentration on particle deposition and release have been successfully modelled by means of semi-empirical relationships (Grolimund and Borkovec 2006, Tosco et al. 2009, Kocur et al. 2013) or by defining the detachment coefficient as a step function of the water IS (Lenhart and Saiers 2003, Becker et al. 2015). Becker et al. (2015) proposed a modified version of the 3D numerical code SEAWAT (Langevin et al. 2008), where the dependency on IS is expressed by a step function which enables particle detachment when IS is under a threshold value and the particle-porous medium interaction energies become more repulsive. Although this approach can be satisfactory when applied to oil reservoirs, where IS spans over a wide range of values up to favorable attachment conditions, it may not be sufficiently accurate in the range of IS variations typical of natural groundwater, where a continuous model would provide more accurate results. Tosco et al. (2009) proposed a set of constitutive equations to model the IS-dependent variation of the attachment and detachment coefficients and of the maximum blocking concentration:

$$k_{a,i}(c_t) = \frac{k_{a\infty,i}}{1+\left(\frac{CDC_i}{c_t}\right)^{\beta_{a,i}}} \qquad (3)$$

$$k_{d,i}(c_t) = \frac{k_{d0,i}}{1+\left(\frac{c_t}{CRC_i}\right)^{\beta_{d,i}}} \qquad (4)$$

$$-\frac{1}{A_2(c_t)} = S_{max,i}(c_t) = \gamma_{s,i} c_t^{\beta_{s,i}} \qquad (5)$$

where subscript *i* refers to the i-th interaction site, subscripts *a* refers to attachment and *d* to detachment. The terms $k_{a\infty,i}$, CDC_i, $\beta_{a,i}$, $k_{d0,i}$, CRC_i, $\beta_{d,i}$, $\gamma_{s,i}$ and $\beta_{s,i}$ are empirical coefficients determined through fitting procedures. c_t is the pore water ionic strength, which is here modelled as a conservative solute solely prone to advection and dispersion. A numerical solution to the coupled eq. (1-5) in 1D domains is provided in MNMs (Tosco and Sethi 2009).

The literature reports several studies investigating the relationship between groundwater velocity and deposition/release of NPs (Ryan and Elimelech 1996, Bradford and Torkzaban 2008, Bedrikovetsky et al. 2011). Under unfavorable deposition conditions, the intensification of the drag forces acting on the particles due to an increase of the flow velocity generally results in enhanced detachment (Li et al. 2005). The models used to describe the influence of flow velocity on the kinetic coefficients are commonly based on the concepts of single collector efficiency (Yao et al. 1971, Logan et al. 1995), for the attachment coefficient, and drag force (Li et al. 2005), for the detachment coefficient. However, these relationships are obtained under conditions that are very different from those typical of experimental or field applications (e.g. single collector, no release, no concurrent phenomena, etc.). In a previous work, Tosco et al. (2014a) proposed a modified formulation of the deposition and release parameters which can be extended to usual field conditions:

$$k_{a,i}(V) = \frac{3}{2}\frac{(1-\epsilon)}{\epsilon d_s} C_{a,i}\eta_0 V \qquad (6)$$

$$k_{d,i}(V) = C_{d,i}\mu V \qquad (7)$$

where μ [M L^{-1} T^{-1}] is the carrier fluid viscosity, V is the modulus of the effective velocity of the pore fluid [L T^{-1}], η_0 is the single collector efficiency [-], d_s [L] is the average diameter of the porous medium grains, $C_{a,i}$ [-] and $C_{d,i}$ [T M^{-1}] are empirical parameters to be determined from fitting of experimental data, and include all the other phenomena not explicitly considered here (dependency on IS, pH, etc.). A numerical solution to eq. (1-2) coupled with eq. (6-7) is provided in MNMs for radial domains (Tosco et al. 2014a).

Following the above-mentioned approaches, in this work a new formulation of the attachment and detachment coefficients is proposed accounting for the simultaneous effects of pore water velocity and ionic strength. To this purpose, the dependency of the empirical parameters $C_{a,i}$ and $C_{d,i}$ on the ionic strength has been explicitly expressed by coupling eq. 3-4 with eq. 6-7:

$$k_{a,i}(V, c_t) = \frac{3}{2}\frac{(1-\epsilon)}{\epsilon d_s}\frac{C'_{a,i}}{1+\left(\frac{CDC_i}{c_t}\right)^{\beta_{a,i}}}\eta_0 V \qquad (8)$$

$$k_{d,i}(V, c_t) = \frac{C'_{d,i}}{1+\left(\frac{c_t}{CRC_i}\right)^{\beta_{d,i}}}\mu V \qquad (9)$$

where $C'_{a,i}$ [-] and $C'_{d,i}$ [T M^{-1}] are fitting parameters which embed all the other phenomena not explicitly considered here.

Since no models are reported in the literature describing the dependency of the maximum concentration of retained particles on the solid phase, s_{max}, on the flow velocity, eq. (5) was adopted here.

For the calculation of the single-collector efficiency, according to Tosco et al. (2014a), the formulation of Yao et al. (1971) is here selected for its simplicity:

$$\eta_0 = \eta_I + \eta_D + \eta_G = \frac{3}{2}\left(\frac{d_c}{d_s}\right)^2 + 4.04 N_{Pe}^{-\frac{2}{3}} + \frac{V_s}{V} \qquad (10)$$

where η_I, η_D and η_G are the removal efficiency due to interception, diffusion and gravity. d_c is the diameter of the colloidal particles [L], V_s is the modulus of the sedimentation rate of the particles in the pore fluid [L T^{-1}], and N_{Pe} is the Peclet number of the particles [L^2T].

In order to overcome the limitations of the single-collector efficiency proposed by Yao (e.g. values greater than one under certain ranges of parameters, negligible particle size, independence from porosity), other more complex formulations can be adopted. Messina et al. (2015) recently proposed a novel total flux normalized correlation equation η_{N_MMS} for predicting single-collector efficiency under a broad range of conditions. It accounts for mutual interaction of concomitant transport mechanisms (i.e. advection, gravity and Brownian motion) and for finite size of the particles (steric effect), and is implemented in MNM3D and MNMs together with the one from Yao.

4.2 3D numerical tool: MNM3D

The kinetic models described above were implemented as user-defined reaction modules within the RT3D code (Clement 1997, Clement et al. 1998). RT3D is a computer code that solves the coupled partial differential equations describing the reactive transport of multiple mobile and/or immobile dissolved species in three-dimensional saturated groundwater systems. Assuming that the dilute concentration of NPs suspended in water would have a negligible influence on the flow field, the transport equations implemented in RT3D can be extended also to the transport of colloidal particles.

MNM3D is composed by four different packages that can be alternatively selected according to the phenomena that must be introduced into the simulation: particle transport with reversible linear or non-linear attachment kinetics (eq. 1-2), IS-dependent transport (eq. 1-5), velocity-dependent transport (eq. 1-2, 6-7, 10), coupled IS- and velocity-dependent transport (eq. 1-2, 5, 8-10). In addition to the general kinetic formulation of the colloid deposition (eq. 2), MNM3D also implements the random sequential adsorption model (Johnson and Elimelech 1995) to describe blocking of the sorption site.

In MNM3D, particles in liquid and solid phase are implemented as distinct species, whose concentrations are correlated by means of kinetic relationships. In this work, a two-site deposition model is adopted (eq. 2), thus leading to a total of four individual species, namely one for particles in liquid phase, two for particles in the solid phase, and one for salt concentration in pore water (see paragraph 4.1). Additional modifications to the core of the code were necessary in order to support the dependency of the kinetic

coefficients on the flow velocity. The velocity field provided by MODFLOW (McDonald and Harbaugh 2003), or other numerical codes, is a multi-dimensional array of velocity values at the cell interfaces, which is natively used by RT3D for the calculation of the advection contribution to the transport. In MNM3D, these data are linearly interpolated to calculate the modulus of the velocity vectors at the center of the cells and compute the velocity-dependent deposition and release coefficients (Eq. 6-7-8-9). To the authors' knowledge, MNM3D is the first 3D numerical code embedding a specific routine for the continuous calculation, cell by cell and at the time-step level (for transient flow simulations), of the attachment and detachment kinetics.

The generation of the input files for MNM3D and the post-processing of its output was performed in Matlab. However, MNM3D can be easily implemented in any other open-source or commercial graphical interface where RT3D is already supported. The partial differential equations system was solved using the TVD (total variation diminishing) method (Leonard 1991).

In order to validate the formulations of ionic strength- and velocity-dependent colloid transport of eq. (3-9), particle transport simulations in one dimensional Cartesian and radial coordinates were performed in MNM3D and compared to the results obtained in MNMs under the same scenarios. The results of the two software were compared for different interaction kinetics in a wide range of injection flow rates, ionic strength (both in transient and constant IS conditions) and kinetic coefficients values, always providing comparable results, with R^2 values always equal or higher than 0.999, thus proving the correct implementation of colloid transport equations (1-10) in MNM3D.

4.3 Column transport tests of graphene oxide

A suspension of Single Layer Graphene Oxide (SLGO Grade 4, Cheap Tubes, U.S., nominal size 300-800 nm) was prepared dispersing SLGO powder in DI water at a concentration of 50 mg/l. The suspension was then dispersed applying three cycles of probe sonication (UP200s Hielsher Untrasound Technology, Germany), each including 10 mins at 50% of maximum power followed by 2 mins stop. Prior each column test, the SLGO suspension was diluted to a particle concentration of 10 g/l. NaCl was added to modify IS of the SLGO dispersions and of flushing solutions. Depending on the test, a concentration of NaCl equal to 0 mM, 10 mM, 20 mM, 35 mM was used. $NaHCO_3$ (0.1 mM) was added as buffer to all suspensions and solutions used in the tests.

SLGO was injected in a chromatographic column with an inner radius of 8 mm, wet-packed with coarse quartz sand (Dorsilit n.7, Dorfner, nominal average grain size d_S = 0.87 mm) at a total length of 11.2(±0.1) cm. Column transport tests were performed following the experimental protocol detailed in Tosco et al. (2012). After packing, columns were flushed for at least 5 prove volumes (PVs) with buffered DI water. All

column tests were carried out at constant flow rate of $1.56 \cdot 10^{-8}$ m^3/s, resulting in a Darcy velocity of $7.76 \cdot 10^{-5}$ m/s, and included the following steps (all performed at constant IS):

- pre-flushing of the column with particle-free buffered NaCl solution (5 PVs);
- SLGO injection (5.5 PVs);
- flushing with particle-free buffered NaCl solution (5.5 PVs).

For the test at 10 mM, a further flushing step was applied, injecting buffered DI water with no NaCl for 5 PVs to promote particle release. The results of this test were used to verify the validity of equations (3-5) under transient ionic strength, as discussed in paragraph 5.2.1.

Salt and particle concentration were continuously monitored at column inlet and outlet with optical density measurements, using a UV-vis spectrophotometer (Specord S600, Analytik Jena, Germany) equipped with flow-through quartz cells with 5 mm light path (Hellma, Germany) at a measurement frequency of 10 s. Salt and SLGO concentrations were monitored at a wavelength of 198.5 nm and 250 nm, respectively.

A tracer (NaCl) injection test was performed on each column (data not reported). Salt breakthrough curves were inverse-fitted using MNMs to determine effective porosity and dispersivity, resulting in an average effective porosity of 0.45(±0.04) and an average dispersivity of $6.17(\pm 0.68) \cdot 10^{-4}$ m.

5 Results and discussion

5.1 Modeling CARBO-IRON® injection in a 2D domain

The injection of CARBO-IRON® particles in a 2D pilot scale flume (Bleyl et al. 2012, Mackenzie et al. 2012, Giannelli et al. 2014, Giannelli et al. 2015) was simulated using MNM3D, solving eq. (1-2,6-7,10). The test was carried out at the VEGAS facility (University of Stuttgart, Germany) as part of the EU research project NanoRem. A container of 1.0x0.12x0.7 m (LxWxH) filled with homogeneous quartz sand (Dorfner, Germany) simulating a confined aquifer was used for the injection. A suspension of CARBO-IRON® particles at a concentration C_{CI}=20 g/l, stabilized by addition of Carboxymethil cellulose (C_{CMC}=4 g/l) was injected in the central part of the domain through 4 delivery points for 48 minutes (Figure 1).

Table 1 Model parameters used for the simulation of the CARBO_IRON® injection in the pilot scale flume. Fitted parameters are identified by the symbol (*)

Flow rate	m^3/s	$1.30 \cdot 10^{-6}$
Injected concentration	g/l	20
Injection time	min	48
Longitudinal dispersivity	m	0.05
Effective porosity	-	0.34
d_{50} sand	m	$6.0 \cdot 10^{-4}$
Carbo-Iron® density (wet particles)	kg/m^3	1700

Particles diameter	nm	800
$C_a^{(*)}$	-	3.5
$C_d^{(*)}$	-	10

The experimental domain was discretized in MNM3D using a regular grid of 100x1x70 (LxWxH) cells. Equal constant head boundary conditions were imposed at the right and left outlets of the container to ensure no base flow. The four injection points were modeled as two vertical wells screened in correspondence to the delivery points. The inverse modeling of column transport tests performed before the 2D injection indicated that CARBO-IRON® retention onto the sand can be modeled assuming a single-site interaction with linear reversible attachment (data not reported). Ionic strength was assumed constant all over the domain for the entire experiment. As a consequence, the equations (1-2, 6-7, 10) were solved in MNM3D, determining the values of C_a and C_d (eq. 6-7) which match the experimental results. To this aim, the simulated maps of total particle concentration (retained and suspended particles) were compared to the images of the flume after 7 and 34 mins of NP injection (Figure 1). The simulated contour line corresponding to a total concentration of CARBO-IRON® nanoparticles equal to 7 g/l (white line in Figure 1C-D-E-F) was chosen to reproduce the edge of the plume (black) visible through the glass wall of the container (Figure 1A-B). This concentration was selected based on experimental results of similar tests performed in flume tanks (data not reported), where the analytical determination of the particle concentration retained on the solid phase identified 7 g/l as the threshold concentration above which particles can clearly imaged in pictures. Figure 1A-B reports the experimental results after 7 and 34 minutes of injection. In Figure 1C-D they are compared to the simulated plumes of CARBO-IRON®, while in Figure 1E-F a comparison with a simulated injection of a tracer in the same operative conditions is shown. The values of the coefficients C_a and C_d were determined by visually matching the 7 g/l simulated contour line to the experimental plume edge on Figure 1C-D. The fitted coefficients and the other model parameters are summarized in Table 1.

The modeled plume reproduces well the experimental one, catching the shape of the experimental spreading area with a good level of approximation. The partial asymmetry observed in the experimental data is due to a slightly higher injection rate associated to the injection points located in the left part of the flume. Comparing the simulation results of particle (Figure 1C-D) and tracer (Figure 1E-F) transport, it is evident that the velocity-dependent attachment implemented in MNM3D better reproduces the retarded transport of the CARBO-IRON® particles due to the interaction with the porous medium. During the first stages of the injection, plumes C and E show a similar spreading area, even though the concentration distribution seems to be more realistic in C, where the particles are retained very close to the injection well. After a longer period, Figure 1D better reproduces the particle behavior both in terms of spreading area, which is overestimated in Figure 1F, and expected concentration distribution.

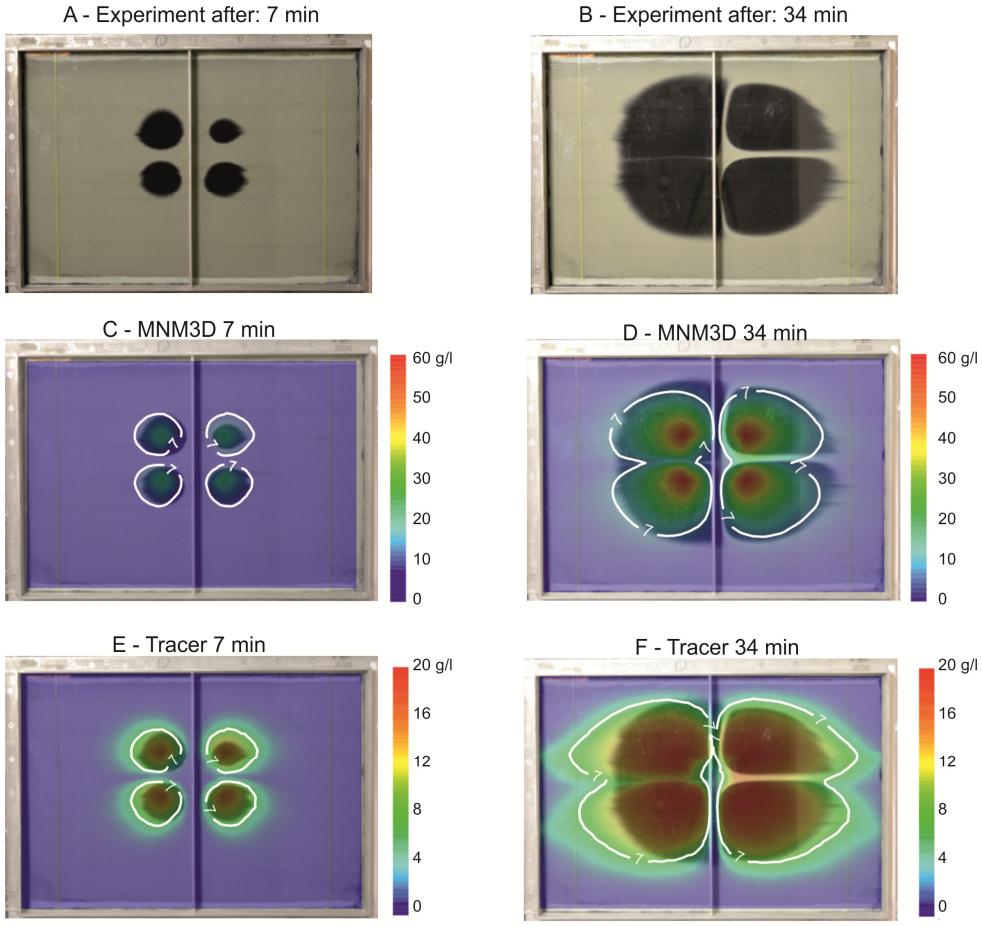

Figure 1 Spreading area of CARBO-IRON® concentration (front view, courtesy of VEGAS) after 7 (A) and 34 (B) minutes from the start of the particle injection. Visual comparison between experimental (black plume) and simulated (colored) results of nanoparticle transport (C, D) and tracer transport (E, F).

The fitted values of C_a and C_d (3.5 and 10, respectively) are of the same order of magnitude of those previously determined by the authors (Tosco et al. 2014a) for zerovalent iron microparticles stabilized with guar gum (2.01 and 0.78 for C_a and 31.35 for C_d). This finding, along with the overall good quality of the matching between experimental and modeled plume, suggests that the model equations (1-2,6-7,10), can correctly describe the transport of CARBO-IRON® in 2D domains in the presence of strong spactial variations of flow velocity. This is particularly relevant since eq. (6-7) were developed for significantly different colloidal systems, namely monodispersed zerovalent iron microspheres, and validated against experiments performed in simpler domains (i.e. column transport tests, see (Tosco et al. 2014a)).

5.2 Simulation of long-term release of graphene oxide in an aquifer system

In the last part of this work the applicability of colloid transport equations described in paragraph 4.1 was tested for SLGO, and applied to simulate the long-term transport of graphene oxides released from a

leaching industrial tank in a contaminated site under space- and time-variable ionic strength. The kinetic parameters controlling SLGO interaction with the porous medium and the associated coefficients were derived from the laboratory column transport tests using MNMs, and then used for the predictive simulations of SLGO transport using MNM3D in a complex aquifer system, following this procedure:

- The experimental breakthrough curves of SLGO column tests were least-squares fitted using MNMs, assuming a single-site reversible blocking deposition (i.e. the coupled equations 1-2 are solved, with $A = -\frac{1}{s_{max}} < 0$, $B = 1$). For each test, a set of parameters k_a, k_d, s_{max} was determined.
- The trend of k_a, k_d, s_{max} as a function of ionic strength was fitted to eq. (3-5) to determine the model parameters ($k_{a\infty}$, CDC, $\beta_{a,i}$, k_{d0}, CRC, β_d, γ_s and β_s).
- The predictive efficacy of the coupled model eqs. (1-5) was tested comparing the experimental results of the extended test at 10 mM (i.e. with final flushing at lower DI) against a predictive simulation of SLGO transport under variable ionic strength under the same conditions (without any further fitting of the coefficients).
- The validated coefficients of eq. (3-5) were included in eq. (8-9) and used for the large-scale simulation of SLGO release and transport in an aquifer system.

5.2.1 Column transport tests for SLGO nanoparticles

The experimental breakthrough curves of column transport tests of SLGO injected in sand-packed columns at constant ionic strength (0.1, 10, 20 and 35 mM) are reported in Figure 2a. The particles resulted extremely mobile in buffered DI water, while in the presence of NaCl a significant retention is observed. Particle deposition increases with increasing ionic strength, consistently with the typical behavior of colloidal particles, and with previous results reported specifically for GO in the literature (Liu et al. 2013a, Zhao et al. 2014, Sun et al. 2015).

The experimental data were then least-squares fitted using MNMs, assuming a single-site reversible blocking deposition. The modeled breakthrough curves are reported in Figure 2a as black lines, and show a good agreement with the experimental data, thus suggesting that the selected attachment/detachment model is correct. The fitted coefficients k_a, k_d and s_{max} are reported in Figure 2b (color symbols) and Table 2 (numerical values), along with R^2 values, which are above 0.98 in all cases.

The trend of the attachment/detachment coefficients with changing ionic strength, evidenced in Figure 2b, is consistent with those previously observed for other particles, and in particular for latex microspheres (Tosco et al. 2009): the attachment rate k_a increases with increasing ionic strength, while the detachment rate decreases with a similar but opposite trend. Also the maximum concentration of particles retainable

onto the solid phase s_{max} increases with ionic strength, even though changes are more limited and span over one order of magnitude, contrary to k_a and k_d. The observed trend of the three coefficients was consequently modeled using eq. (3-5) (color lines in Figure 2b; the numerical values of the fitted coefficients in eq. (3-5) are reported in Paragraph 2 of the Supporting Information).

The model equations satisfactorily fit the point values. This finding is of particular interest since the relationships of eq. (3-5) were previously derived following a semi-empirical approach for ideal colloids, namely latex microspheres (Tosco et al. 2009), but to the authors knowledge their validity was never tested before for graphene oxide, nor more in general for non-spherical particles. As a consequence, apart from providing a relationship to model the dependency of attachment/detachment parameters from ionic strength for this specific application, this finding suggests that eq. (3-5) have a general validity and can be potentially applied to any colloidal system.

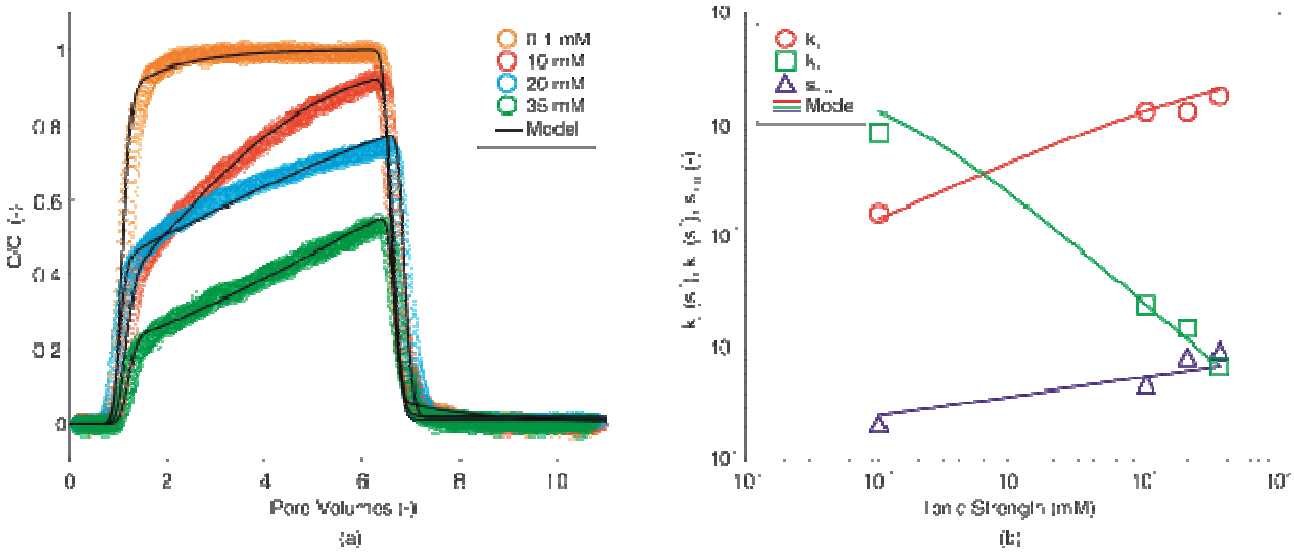

Figure 2 (a) Experimental (color points) and modeled (black lines) breakthrough curves of SLGO transport tests at different NaCl concentrations; (b) least-squares fitted kinetic coefficients (k_a, k_d, s_{max}) as a function of ionic strength for each test (color points), and the corresponding modeled curves of eq. (3-5) (color lines).

Table 2 Attachment rate (k_a), detachment rate (k_d) and maximum concentration of retained particles (s_{max}) obtained from least-squares fitting of breakthrough curves of SLGO column tests, and R^2 coefficient.

Ionic strength	mM	0.1	10	20	35
k_a	s^{-1}	$1.64 \cdot 10^{-4}$	$1.33 \cdot 10^{-6}3$	$1.31 \cdot 10^{-3}$	$1.79 \cdot 10^{-3}$
k_d	s^{-1}	$8.60 \cdot 10^{-4}$	$2.49 \cdot 10^{-6}5$	$1.54 \cdot 10^{-5}$	$7.06 \cdot 10^{-6}$
s_{max}	-	$2.17 \cdot 10^{-6}$	$4.98 \cdot 10^{-6}$	$7.5 \cdot 10^{-6}$	$9.69 \cdot 10^{-6}$
R^2	-	0.9900	0.9899	0.9952	0.9884

To further prove the validity of the adopted model for IS-dependent transport of SLGO, the test performed at 10 mM NaCl was extended including an additional flushing step at lower ionic strength (namely, DI with

0.1 mM $NaHCO_3$) to promote the release of reversibly deposited particles (Figure 3). Decreasing ionic strength during flushing resulted in a peak release of retained SLGO, as expected from the observed behavior of other colloidal particles (Tosco et al. 2009). The peak was very well captured by the model equations (1-5): for this simulation, the coefficients of eq. (3-5) determined by fitting the trends of k_a, k_d and s_{max} of the tests at constant ionic strength (Figure 2b) were used for a predictive (direct) simulation, without any further fitting nor adjustment of the coefficients. The good agreement between experimental and modeled breakthrough curves further confirm the suitability of eq. (3-5) to model SLGO transport under variable ionic strength.

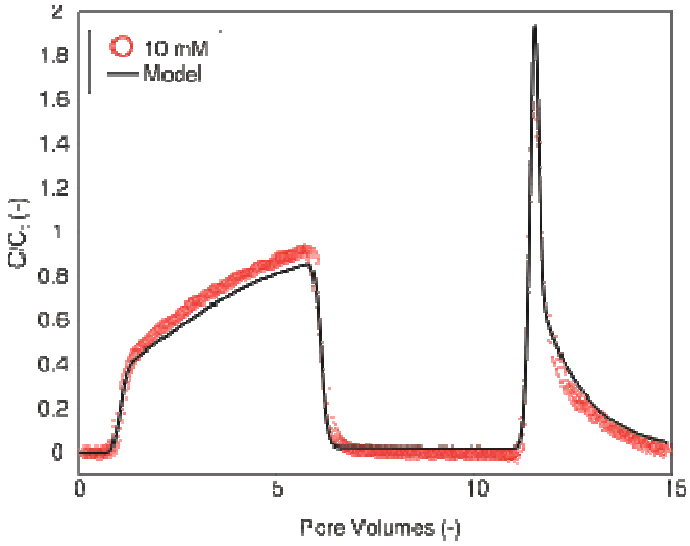

Figure 3 (a) Experimental (red points) and modeled (black line) breakthrough curves of SLGO transport test under variable ionic strength. The test included pre-flushing with NaCl 10 mM (not reported), particle injection with NaCl 10 mM (5.5 PVs), a first flushing with NaCl 10 mM (5.5 PVs) and a second flushing with DI+$NaHCO_3$ 0.1 mM (5 PVs).

5.2.2 Modeling SLGO release and transport in a heterogeneous aquifer system

The results of the modeling of SLGO column transport tests were used to simulate graphene oxide release and transport in a heterogeneous aquifer. SLGO transport in the 3D domain was simulated using MNM3D, taking into account the concurrent influence of space- and time- variable IS and flow velocity on the transport kinetics. In particular, the information on the influence of ionic strength was derived from the modeling of column transport tests using MNMs, discussed in the previous paragraph. The velocity-dependent formulation of eq. (6-7) was assumed valid for SLGO. The ionic strength was modeled as a tracer solute, c_t, subject to advection and dispersion (no sorption nor degradation), influencing the SLGO

attachment/detachment rate and the maximum concentration in the solid phase. As a consequence, the particle transport was modeled by the following set of coupled transport equations:

$$\begin{cases} \frac{\partial}{\partial t}(\epsilon c_t) + \frac{\partial}{\partial x_i}(q_i c_t) - \frac{\partial^2}{\partial x_i^2}\left(\epsilon D_{ij} c_t\right) - q_s c_t = 0 \\ \frac{\partial}{\partial t}(\epsilon C) + \frac{\partial}{\partial t}(\rho_b S) + \frac{\partial}{\partial x_i}(q_i C) - \frac{\partial^2}{\partial x_i^2}\left(\epsilon D_{ij} C\right) - q_s C = 0 \\ \frac{\partial}{\partial t}(\rho_b S) = \epsilon k_a \left(1 - \frac{\mathrm{S}}{\mathrm{S_{max}}}\right) C - \rho_b k_d \mathrm{S} \end{cases} \qquad (11)$$

where

$$\begin{cases} k_a(V, c_t) = \frac{3}{2}\frac{(1-\epsilon)}{\epsilon d_s}\frac{C'_a}{1+\left(\frac{CDC}{c_t}\right)^{\beta a}}\eta_0 V \\ k_d(V, c_t) = \frac{C'_d}{1+\left(\frac{c_t}{CRC}\right)^{\beta_d}}\mu V \\ S_{max}(c_t) = \gamma_s c_t^{\beta_s} \end{cases} \qquad (12)$$

Eq. (10) was adopted to calculate η_0. The values of the coefficients CDC, CRC, γ_s, β_a, β_d, β_s, are those obtained from the modeling of the column tests, while C'_a and C'_d were calculated from $C_{a,0}$ and $C_{d,\infty}$ of the column tests by equating eq (3-4) to eq. (8-9), respectively, and resulted equal to C'_a = 2.41 and C'_d = $1.43 \cdot 10^5$ s/kg.

The SLGO transport was simulated in a multilayer unconfined aquifer contaminated by a leaching tank. The model domain was modified from the case study presented by Rolle et al. (2008). The aquifer consists of three layers (Figure 4): an upper and a lower homogeneous sandy layers (K_h=$6.9 \cdot 10^{-4}$ m/s, green area in Figure 4), and an intermediate clayey-silty layer (K_h=$1 \cdot 10^{-10}$ m/s, blue area in Figure 4). A discontinuity in the upper and intermediate layers is represented by the relic bed of a river, consisting of a highly permeable sandy-gravel area (grey portion in Figure 4). Moreover, a lower permeability region (blue area) is also present in the upper layer. Water flow is from left to right (blue arrow in Figure 4) and was obtained imposing two constant head boundary conditions. The background ionic strength is 2 mM in the upper layer and 1.5 mM in the intermediate and lower ones. The source of SLGO is represented by a 17x30 m leaching tank containing waste water with a SLGO concentration of 100 mg/l and a water salinity of 350 mM. The release into the aquifer is continuous and corresponds to approximately 1.4 m^3/day.

The domain has a total size of 1000 x 1400 x 24 m, discretized in 247800 cells. In the vertical direction, the three aquifer levels were discretized in 5 cells each, resulting in a total of 15 layers in the model domain. A uniform cell spacing of 10 and 8.5 m was adopted, respectively, in the longitudinal and transversal directions, resulting in 140x118 cells per layer. The steady state simulation of the groundwater flow field was performed using the finite difference code MODFLOW-2000 (Harbaugh et al., 2000). The transport of

the dissolved salt was simulated assuming no sorption nor degradation (i.e. as a tracer). Tracer and SLGO release were assumed to start at the same time, and were both solved in transient conditions using MNM3D.

In this scenario, the salinity contrast between the upper and the lower aquifers and between the leachate and the groundwater is expected to play a crucial role in the particle transport: colloids usually exhibit a limited mobility at high IS (as for leachate) and therefore a significant retention close to the release point is expected. However, at larger distances, when the leachate is diluted by the background flow and particles reach the less saline layer, a higher mobility is envisioned.

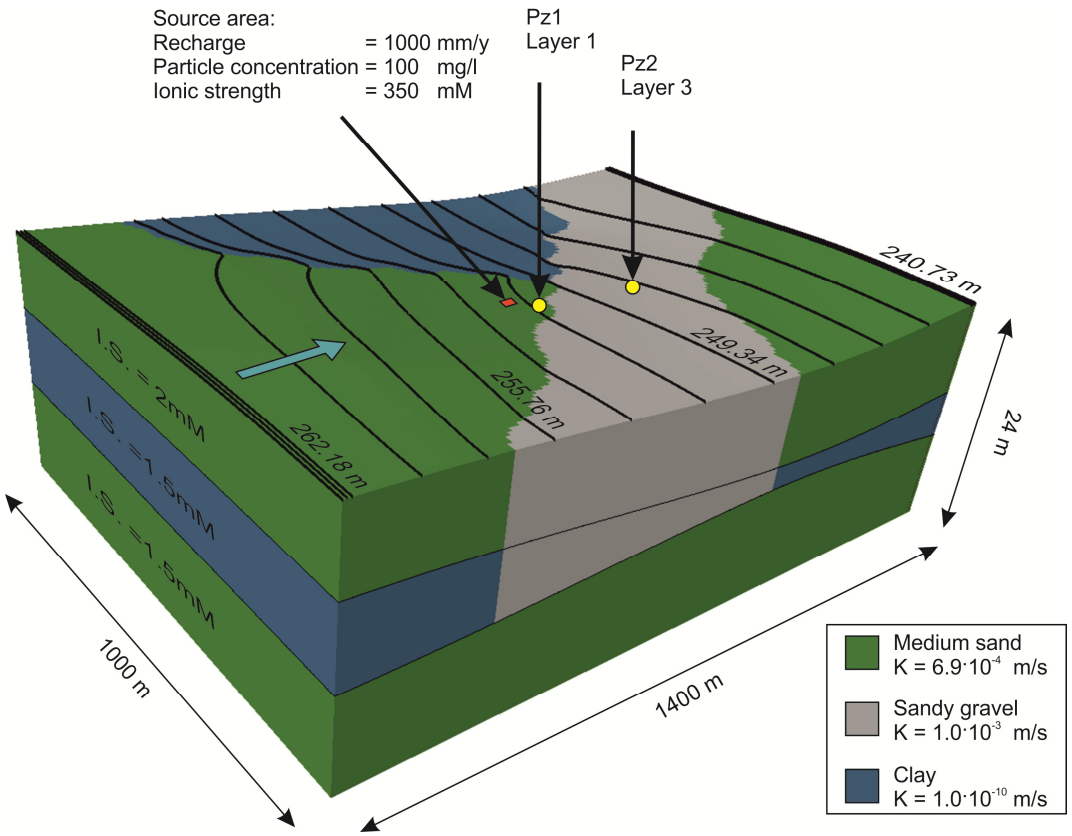

Figure 4 Conceptual model, boundary conditions and flow field of the simulated contaminated aquifer

Two different scenarios of particle emission were simulated to highlight the effect of ionic strength and flow velocity on the behavior of nanoparticles: a) particle release and transport with dependency on flow velocity and ionic strength (i.e. following the complete set of eq. (11-12)), and b) transport with k_a, k_d and s_{max} constant over space and time. In the second case, the three coefficients were calculated using equations (12) for a constant ionic strength of 3.8 mM (i.e assuming that particle transport kinetics are equal to those registered directly below the source area) and a constant velocity equal to the average velocity of the aquifer system (calculated applying the Darcy law to the horizontal hydraulic conductivity of the medium-sand layer and to the average hydraulic gradient).

Figure 5 reports the particle plume for scenario a and the evolution in time of concentration at two monitoring points, Pz1 and Pz2 (Figure 5a-b), located respectively at 40 m (in the upper layer) and 220 m (in the lowest layer) from the center of the contamination source. At the bottom of the figure, the ionic strength profiles at steady state along the plume axis adopted in the simulation of scenarios a and b are also reported. The SLGO nanoparticles resulted significantly more mobile in scenario a than in scenario b, where particles do not even reach the lower aquifer. The assumption of constant kinetic coefficients, obtained using punctual value of velocity and ionic strength and neglecting the effect of their variation inside the domain, may therefore not be adequate to properly foresee the particle behavior. In particular, it may lead to a significant underestimation of the particle travel distance (Figure 5a-b) toward a possible receptor, especially at larger distances from the contamination source. On the contrary, when variations of groundwater IS are taken into account in the model, particles mobility proves to be significantly enhanced because of the space-variable attachment and detachment coefficients, resulting in a more realistic behavior. The comparison of the release scenarios a and b therefore suggests that it is very important not to neglect the effect of spatial and temporal variations of the groundwater IS and velocity, and MNM3D can represent in this sense a useful tool for the long term prediction of particle fate.

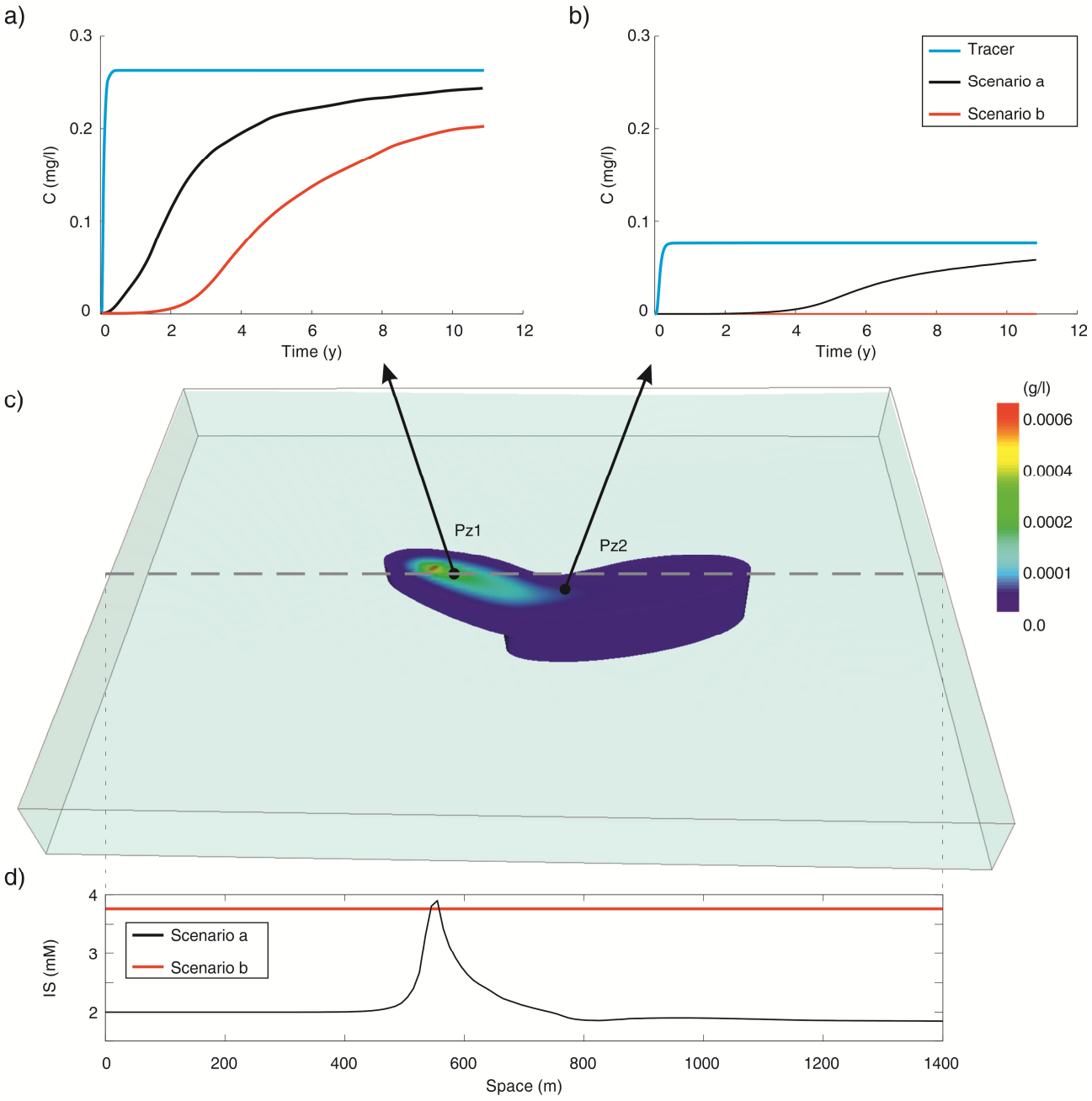

Figure 5 Simulation of particle transport after 2.5 years of continuous release: a) particle concentration vs time at Pz1; b) particle concentration vs time at Pz2; c) particle plume simulated under transient ionic strength conditions (scenario a); d) steady state profile of ionic strength along the plume axis for scenarios a and b.

6 Conclusions

In this work, the large-scale transport of carbon-based nanomaterials with a significant environmental relevance, namely CARBO-IRON® and single layer graphene oxide, was successfully simulated. A new numerical tool, MNM3D, was developed based on RT3D for the simulation of nanoparticle transport in 3D domains, and applied to this purpose. The successful simulation of the flume experiment suggested that the modeling approach and its numerical solution provided by MNM3D can correctly describe the transport

of CARBO-IRON® and consequently are suitable to simulate the injection of these particles in complex scenarios. Similarly, the results of the modeling of column tests for SLGO indicate that the modeling approach is suitable also for the simulation of the transport of particles, namely graphene sheets, which are extremely different in shape and surface properties compared to natural and engineered NPs typically studied in column transport tests. This finding allowed the final application of MNM3D to the simulation of long-term mobility of SLGO in a complex 3D scenario.

MNM3D can predict the kinetic transport of micro- and nanoparticles in groundwater and their physico-chemical interaction with the solid matrix, accounting for simultaneous dependency of the attachment and detachment kinetics on the groundwater ionic strength and velocity. It can be applied either for short term evaluation of particles distribution around one or more wells, such as in case of groundwater remediation via engineered particles injection, and long term particle spreading prediction, e.g. fate of particles release from a landfill. With respect to the other available simulation tools for nanoparticles transport, MNM3D can be applied to more realistic domains, with complex geometries and boundary conditions. Inhomogeneity of the porous medium and of the particle-soil interactions can be taken into account by implementing space-variable hydrodynamic, transport and kinetic parameters. Moreover, MNM3D can be easily implemented in many open-source and commercial graphical interface which already support the well-known RT3D numerical code it is based on. Therefore, MNM3D overcomes many limitations and approximations of the other simplified numerical codes and offers the opportunity to fill the gap between the controlled conditions of laboratory tests and the more complex scenarios typical of field-scale applications.

7 Acknowledgments

The work was co-funded by the EU research project NanoRem (FP7, Grant Agreement n. 309517). The authors want to thank Dr. Jürgen Braun, Giulia Giannelli (VEGAS - University of Stuttgart) and Dr. Katrin Mackenzie (Helmholtz Centre for Environmental Research, Leipzig) for providing the experimental data of the pilot-scale injection of CARBO-IRON® nanoparticles, and Dr. T. Prabhakar Clement who kindly provided the source code of RT3D.

8 References

Becker, M.D., Wang, Y., L. Paulsen, J., Song, Y.Q., Abriola, L.M. and Pennell, K.D. (2015) In situ measurement and simulation of nano-magnetite mobility in porous media subject to transient salinity. Nanoscale 7(3), 1047-1057.

Bedrikovetsky, P., Siqueira, F., Furtado, C. and Souza, A. (2011) Modified Particle Detachment Model for Colloidal Transport in Porous Media. Transport in Porous Media 86(2), 353-383.

Bekhit, H.M. and Hassan, A.E. (2007) Subsurface contaminant transport in the presence of colloids: Effect of nonlinear and nonequilibrium interactions. Water Resources Research 43(8).

Bleyl, S., Kopinke, F.D. and Mackenzie, K. (2012) Carbo-Iron ®-Synthesis and stabilization of Fe(0)-doped colloidal activated carbon for in situ groundwater treatment. Chemical Engineering Journal 191, 588-595.

Bosch, J., Heister, K., Hofmann, T. and Meckenstock, R.U. (2010) Nanosized Iron Oxide Colloids Strongly Enhance Microbial Iron Reduction. Applied and Environmental Microbiology 76(1), 184-189.

Bradford, S.A., Kim, H.N., Haznedaroglu, B.Z., Torkzaban, S. and Walker, S.L. (2009) Coupled factors influencing concentration-dependent colloid transport and retention in saturated porous media. Environmental Science and Technology 43(18), 6996-7002.

Bradford, S.A. and Torkzaban, S. (2008) Colloid transport and retention in unsaturated porous media: A review of interface-, collector-, and pore-scale processes and models. Vadose Zone Journal 7(2), 667-681.

Braunschweig, J., Bosch, J. and Meckenstock, R.U. (2013) Iron oxide nanoparticles in geomicrobiology: from biogeochemistry to bioremediation. New Biotechnology 30(6), 793-802.

Chrysikopoulos, C.V., Syngouna, V.I., Vasiliadou, I.A. and Katzourakis, V.E. (2012) Transport of Pseudomonas putida in a 3-D Bench Scale Experimental Aquifer. Transport in Porous Media 94(3), 617-642.

Clement, T.P. (1997) RT3D - A Modular Computer Code for Simulating Reactive Multi-Species Transport in 3-Dimensional Groundwater Aquifers, Pacific Northwest National Laboratory, Richland, WA, USA. PNNL-11720.

Clement, T.P., Sun, Y., Hooker, B.S. and Petersen, J.N. (1998) Modeling multispecies reactive transport in ground water. Ground Water Monitoring and Remediation 18(2), 79-92.

Feriancikova, L. and Xu, S. (2012) Deposition and remobilization of graphene oxide within saturated sand packs. Journal of Hazardous Materials 235–236(0), 194-200.

Giannelli, G., Bleyl, S., Sethi, R. and Braun, J. (2015) Small Flume Experiment for the Transport Evaluation of CARBO-IRON® particles in a confined aquifer, Copenhagen.

Giannelli, G., Sethi, R. and Braun, J. (2014) Small Flume Experiment for the Transport Evaluation of Carbo-Iron Particles in a Confined Aquifer, Darmstadt.

Grolimund, D. and Borkovec, M. (2006) Release of colloidal particles in natural porous media by monovalent and divalent cations. Journal of Contaminant Hydrology 87(3-4), 155-175.

Johnson, P.R. and Elimelech, M. (1995) Dynamics of colloid deposition in porous media. Blocking based on random sequential adsorption. Langmuir 11(3), 801-812.

Johnson, R.L., Nurmi, J.T., O'Brien Johnson, G.S., Fan, D., O'Brien Johnson, R.L., Shi, Z., Salter-Blanc, A.J., Tratnyek, P.G. and Lowry, G.V. (2013) Field-scale transport and transformation of carboxymethylcellulose- stabilized nano zero-valent iron. Environmental Science and Technology 47(3), 1573-1580.

Kanti Sen, T. and Khilar, K.C. (2006) Review on subsurface colloids and colloid-associated contaminant transport in saturated porous media. Advances in Colloid and Interface Science 119(2–3), 71-96.

Katzourakis, V.E. and Chrysikopoulos, C.V. (2014) Mathematical modeling of colloid and virus cotransport in porous media: Application to experimental data. Advances in Water Resources 68, 62-73.

Kocur, C.M., O'Carroll, D.M. and Sleep, B.E. (2013) Impact of nZVI stability on mobility in porous media. Journal of Contaminant Hydrology 145, 17-25.

Langevin, C.D., Thorne, D.T.J., Dausman, A.M., Sukop, M.C. and Guo, W. (2008) SEAWAT Version 4: A Computer Program for Simulation of Multi-Species Solute and Heat Transport, U.S. Geological Survey, Reston, Virginia.

Lanphere, J.D., Luth, C.J. and Walker, S.L. (2013) Effects of Solution Chemistry on the Transport of Graphene Oxide in Saturated Porous Media. Environmental Science & Technology 47(9), 4255-4261.

Lenhart, J.J. and Saiers, J.E. (2003) Colloid Mobilization in Water-Saturated Porous Media under Transient Chemical Conditions. Environmental Science & Technology 37(12), 2780-2787.

Leonard, B.P. (1991) The ULTIMATE conservative difference scheme applied to unsteady one-dimensional advection. Computer Methods in Applied Mechanics and Engineering 88(1), 17-74.

Li, X., Zhang, P., Lin, C.L. and Johnson, W.P. (2005) Role of Hydrodynamic Drag on Microsphere Deposition and Re-entrainment in Porous Media under Unfavorable Conditions. Environmental Science & Technology 39(11), 4012-4020.

Li, X.Q., Elliott, D.W. and Zhang, W.X. (2006) Zero-valent iron nanoparticles for abatement of environmental pollutants: Materials and engineering aspects. Critical Reviews in Solid State and Materials Sciences 31(4), 111-122.

Liu, L., Gao, B., Wu, L., Morales, V.L., Yang, L., Zhou, Z. and Wang, H. (2013a) Deposition and transport of graphene oxide in saturated and unsaturated porous media. Chemical Engineering Journal 229(0), 444-449.

Liu, L., Gao, B., Wu, L., Yang, L., Zhou, Z. and Wang, H. (2013b) Effects of pH and surface metal oxyhydroxides on deposition and transport of carboxyl-functionalized graphene in saturated porous media. Journal of Nanoparticle Research 15(11), 1-8.

Logan, B.E., Jewett, D.G., Arnold, R.G., Bouwer, E.J. and O'Melia, C.R. (1995) Clarification of clean-bed filtration models. Journal of Environmental Engineering 121(12), 869-873.

Mackenzie, K., Bleyl, S., Georgi, A. and Kopinke, F.D. (2012) Carbo-Iron - An Fe/AC composite - As alternative to nano-iron for groundwater treatment. Water Research 46(12), 3817-3826.

Mackenzie, K., Bleyl, S., Kopinke, F.D., Doose, H. and Bruns, J. (2015) Carbo-Iron as improvement of the nanoiron technology: From laboratory design to the field test. Science of the Total Environment.

McDonald, M.G. and Harbaugh, A.W. (2003) The history of MODFLOW. Ground water 41(2), 280-283.

Messina, F., Marchisio, D.L. and Sethi, R. (2015) An extended and total flux normalized correlation equation for predicting single-collector efficiency. Journal of Colloid and Interface Science 446(0), 185-193.

Novoselov, K.S., Fal'Ko, V.I., Colombo, L., Gellert, P.R., Schwab, M.G. and Kim, K. (2012) A roadmap for graphene. Nature 490(7419), 192-200.

O'Carroll, D., Sleep, B., Krol, M., Boparai, H. and Kocur, C. (2013) Nanoscale zero valent iron and bimetallic particles for contaminated site remediation. Advances in Water Resources 51(0), 104-122.

Rolle, M., Clement, T.P., Sethi, R. and Di Molfetta, A. (2008) A kinetic approach for simulating redox-controlled fringe and core biodegradation processes in groundwater: Model development and application to a landfill site in Piedmont, Italy. Hydrological Processes 22(25), 4905-4921.

Ryan, J.N. and Elimelech, M. (1996) Colloid mobilization and transport in groundwater. Colloids and Surfaces A: Physicochemical and Engineering Aspects 107, 1-56.

Saleh, N., Kim, H.-J., Phenrat, T., Matyjaszewski, K., Tilton, R.D. and Lowry, G.V. (2008) Ionic Strength and Composition Affect the Mobility of Surface-Modified Fe0 Nanoparticles in Water-Saturated Sand Columns. Environmental Science & Technology 42(9), 3349-3355.

Šimůnek, J., Van Genuchten, M.T. and Šejna, M. (2008) Development and applications of the HYDRUS and STANMOD software packages and related codes. Vadose Zone Journal 7(2), 587-600.

Sun, Y., Gao, B., Bradford, S.A., Wu, L., Chen, H., Shi, X. and Wu, J. (2015) Transport, retention, and size perturbation of graphene oxide in saturated porous media: Effects of input concentration and grain size. Water Research 68(0), 24-33.

Tiraferri, A., Tosco, T. and Sethi, R. (2011) Transport and retention of microparticles in packed sand columns at low and intermediate ionic strengths: Experiments and mathematical modeling. Environmental Earth Sciences 63(4), 847-859.

Tosco, T., Bosch, J., Meckenstock, R.U. and Sethi, R. (2012) Transport of ferrihydrite nanoparticles in saturated porous media: Role of ionic strength and flow rate. Environmental Science and Technology 46(7), 4008-4015.

Tosco, T., Gastone, F. and Sethi, R. (2014a) Guar gum solutions for improved delivery of iron particles in porous media (Part 2): Iron transport tests and modeling in radial geometry. Journal of Contaminant Hydrology 166(0), 34-51.

Tosco, T., Petrangeli Papini, M., Cruz Viggi, C. and Sethi, R. (2014b) Nanoscale zerovalent iron particles for groundwater remediation: a review. Journal of Cleaner Production 77(0), 10-21.

Tosco, T. and Sethi, R. (2009) MNM1D: A numerical code for colloid transport in porous media: Implementation and validation. American Journal of Environmental Sciences 5(4), 516-524.

Tosco, T. and Sethi, R. (2010) Transport of non-newtonian suspensions of highly concentrated micro- and nanoscale iron particles in porous media: A modeling approach. Environmental Science and Technology 44(23), 9062-9068.

Tosco, T., Tiraferri, A. and Sethi, R. (2009) Ionic Strength Dependent Transport of Microparticles in Saturated Porous Media: Modeling Mobilization and Immobilization Phenomena under Transient Chemical Conditions. Environmental Science & Technology 43(12), 4425-4431.

Tratnyek, P.G. and Johnson, R.L. (2006) Nanotechnologies for environmental cleanup. Nano Today 1(2), 44-48.

Tufenkji, N. and Elimelech, M. (2004a) Correlation equation for predicting single-collector efficiency in physicochemical filtration in saturated porous media. Environmental Science & Technology 38(2), 529-536.

Tufenkji, N. and Elimelech, M. (2004b) Deviation from the classical colloid filtration theory in the presence of repulsive DLVO interactions. Langmuir 20(25), 10818-10828.

Yan, W., Lien, H.-L., Koel, B.E. and Zhang, W.-x. (2013) Iron nanoparticles for environmental clean-up: recent developments and future outlook. Environmental Science: Processes & Impacts 15(1), 63-77.

Yao, K.-M., Habibian, M.T. and O'Melia, C.R. (1971) Water and waste water filtration. Concepts and applications. Environmental Science & Technology 5(11), 1105-1112.

Zhang, W.-x. (2003) Nanoscale Iron Particles for Environmental Remediation: An Overview. Journal of Nanoparticle Research 5(3-4), 323-332.

Zhao, J., Wang, Z., White, J.C. and Xing, B. (2014) Graphene in the Aquatic Environment: Adsorption, Dispersion, Toxicity and Transformation. Environmental Science & Technology 48(17), 9995-10009.